LDPC coded OFDM over the atmospheric turbulence channel

Ivan B. Djordjevic, Bane Vasic, and Mark A. Neifeld

University of Arizona, Department of Electrical and Computer Engineering, Tucson, AZ 85721, USA
ivan@ece.arizona.edu, vasic@ece.arizona.edu, mark@ece.arizona.edu

Abstract: Low-density parity-check (LDPC) coded optical orthogonal frequency division multiplexing (OFDM) is shown to significantly outperform LDPC coded on-off keying (OOK) over the atmospheric turbulence channel in terms of both coding gain and spectral efficiency. In the regime of strong turbulence at a bit-error rate of 10^{-5}, the coding gain improvement of the LDPC coded single-side band unclipped-OFDM system with 64 sub-carriers is larger than the coding gain of the LDPC coded OOK system by 20.2dB for quadrature-phase-shift keying (QPSK) and by 23.4dB for binary-phase-shift keying (BPSK).

OCIS codes: (060.4510) Optical communications; (010.1330) Atmospheric turbulence; (060.4080) Modulation; (060.4230) Multiplexing; (999.9999) Orthogonal frequency division multiplexing; (999.9999) Low-density parity-check (LDPC) codes

References and Links

1. X. Zhu, and J. M. Kahn, "Free-space optical communication through atmospheric turbulence channels," IEEE Trans. Commun. **50**, 1293-1300 (2002).
2. M. A. Al-Habash, L. C. Andrews, and R. L. Phillips, "Mathematical model for the irradiance probability density function of a laser beam propagating through turbulent media," Opt. Eng. **40**, 1554-1562 (2001).
3. X. Zhu, and J. M. Kahn, "Markov chain model in maximum-likelihood sequence detection for free-space optical communication through atmospheric turbulence channels," J. Lightwave Technol. **51**, 509-516 (2003).
4. M.-C. Jeong, J.-S. Lee, S.-Y. Kim, S.-W. Namgung, J.-H. Lee, M.-Y. Cho, S.-W. Huh, Y.-S. Ahn, J.-W. Cho, and J.-S. Lee, "8x10 Gb/s terrestrial optical free-space transmission over 3.4 km using an optical repeater," IEEE Photon. Technol. Lett. **15**, 171-173 (2003).
5. J. A. Anguita, I. B. Djordjevic, M. A. Neifeld, and B. V. Vasic, "Shannon capacities and error-correction codes for optical atmospheric trubulent channels," J. Opt. Net. **4**, 586-601 (2005).
6. R. Van Nee and R. Prasad, *OFDM Wireless Multimedia Communications*, (Artech House, Boston 2000).
7. Y. Wu and B. Caron, "Digital television terrestrial broadcasting," IEEE Commun. Mag. **32**, 46–52 (1994).
8. Q. Pan and R. J. Green, "Bit-error-rate performance of lightwave hybrid AM/OFDM systems with comparison with AM/QAM systems in the presence of clipping impulse noise," IEEE Photon. Technol. Lett. **8**, 278–280 (1996).
9. A. Kim, Y. Hun Joo, and Y. Kim, "60 GHz wireless communication systems with radio-over-fiber links for indoor wireless LANs," IEEE Trans. Commun. Electron. **50**, 517-520 (2004).
10. B. J. Dixon, R. D. Pollard, and S. Iezekiel, "Orthogonal frequency-division multiplexing in wireless communication systems with multimode fiber feeds," IEEE Trans Microwave Theory Tech. **49**, 1404 – 1409 (2001).
11. I. B. Djordjevic, O. Milenkovic, and B. Vasic, "Generalized low-density parity-check codes for Optical Communication Systems," J. Lightwave Technol. **23**, 1939- 1946 (2005).
12. I. B. Djordjevic and B. Vasic, "Nonbinary LDPC codes for optical communication systems," IEEE Photon. Technol. Lett. **17**, 2224-2226 (2005).
13. O. Milenkovic, I. B. Djordjevic, and B. Vasic, "Block-circulant low-density parity-check codes for optical communication systems," J. Sel. Top. Quantum Electron. **10**, 294-299 (2004).
14. R. You and J. M. Kahn, "Average power reduction techniques for multiple-subcarrier intensity-modulated optical signals," IEEE Trans. Commun. **49**, 2164-2171 (2001).
15. H. X.-Yu, E. Eleftheriou, D.-M. Arnold, and A. Dholakia, "Efficient implementations of the sum-product algorithm for decoding of LDPC codes," in Proc. IEEE Globecom 2001 **2**, 1036-1036E (2001).
16. R. Hui, B. Zhu, R. Huang, C. T. Allen, K. R. Demarest, and D. Richards, "Subcarrier multiplexing for high-speed optical transmission," J. Lightwave Technol. **20**, 417-427 (2002).
17. J. G. Proakis, *Digital Communications* (McGraw Hill, Boston 2001).

#79874 - $15.00 USD Received 7 Feb 2007; revised 30 Apr 2007; accepted 30 Apr 2007; published 8 May 2007

18. W. E. Ryan, "Concatenated convolutional codes and iterative decoding," in *Wiley Encyclopedia in Telecommunications*, J. G. Proakis, ed., (John Wiley and Sons, 2003).
19. C.-C. Lin, K.-L. Lin, H.-Ch. Chang, and C.-Y. Lee, "A 3.33Gb/s (1200,720) low-density parity check code decoder," in Proc. ESSCIRC 2005, 211-214 (2005).
20. L. C. Andrews and R. L. Philips, *Laser beam propagation through random media*, (SPIE Optical Engineering Press, 1998).
21. N. Levinson, "The Wiener RMS error criterion in filter design and prediction," J. Math. Phys. **25**, 261-278 (1947).
22. J. Durbin, "Efficient estimation of parameters in moving-average models," Biometrica **46**, 306-316 (1959).
23. A. T. A Wood and G. Chan, "Simulation of stationary Gaussian processes in $[0,1]^d$," J. Comp. Graph. Stat. **3**, 409-432 (1994).

1. Introduction

Due to the high-complexity associated with coherent detection, current free-space optical (FSO) communication systems [1-5] employ intensity modulation with direct detection (IM/DD). Such systems use point-to-point communication between two optical transceivers along a line of sight. For example, a 8×10 Gb/s terrestrial FSO transmission over 3.4 km using an optical repeater was demonstrated in [4]. The IM/DD technique is also used in state-of-the-art fiber-optic communications, and the availability of optical components used in fiber-based systems makes FSO communication a cost-effective solution for high-rate image, voice and data transmission [1-5].

However, an optical wave propagating through the air experiences fluctuations in amplitude and phase due to atmospheric turbulence [1-5]. The atmospheric turbulence is caused by variations in the refractive index of the transmission medium due to inhomogenities in temperature and pressure caused by solar heating and wind. The atmospheric turbulence optical channel has been intensively studied and various models have been proposed to describe turbulence-induced performance degradation and intensity fluctuations [1-3]. The intensity fluctuation, also known as scintillation, is one of the most important factors that degrade the performance of an FSO communication link. Due to constraints on the receiver size, it is not always possible to ensure that the receiver aperture is significantly larger than the turbulent correlation length. In such a case aperture averaging becomes ineffective, and alternative techniques to mitigate the intensity fluctuations are required [1]. These techniques can be placed into two broad categories. Spatial-domain techniques [1] involve diversity detection using multiple receivers, and time-domain techniques [3] adaptively optimize the decision threshold according to the maximum likelihood criterion. When the receiver has knowledge of the joint temporal distribution of intensity fluctuations, maximum-likelihood sequence detection (MLSD) can be employed. MLSD has high computational complexity, and sub-optimal implementations of MLSD such as those based on sub-optimal per-survivor processing (PSP) [3] are more likely to be implemented in practice. At bit-error rate (BER) below 10^{-6} both MLSD and PSP require the electrical signal to noise ratio larger than 20 dB even in the weak turbulence regime. Such signal powers are unacceptably high for many applications, and novel modulation techniques for IM/DD FSO systems are needed. In this paper we show that orthogonal frequency division multiplexing (OFDM) combined with error control coding is a very good modulation format for FSO IM/DD systems.

OFDM [6-9] is a special case of a multicarrier transmission in which a single information-bearing stream is transmitted over many lower rate subchannels. It has been used for digital audio broadcasting [6], high-definition television (HDTV) terrestrial broadcasting [7], in digital subscriber line (DSL) systems [6], in IEEE 802.11, in high-performance LAN type 2 (HIPERLAN/2) and multimedia mobile access communication wireless LANs [6], and has been studied for use in lightwave hybrid AM/OFDM cable systems [8], and in radio over fiber-based networks [9,10]. It is interesting to notice that modern digital TV broadcasting is based on OFDM [7], and that OFDM is intensively studied for wireless applications [6]. Because the FSO link is a cost-effective solution for transmission of high-speed signals, the study of OFDM transmission over the FSO link is becoming increasingly important.

#79874 - $15.00 USD Received 7 Feb 2007; revised 30 Apr 2007; accepted 30 Apr 2007; published 8 May 2007

OFDM uses the fast Fourier transform (FFT) algorithm for modulation and demodulation, and requires no equalization. At the same time it provides high spectral efficiency. These features together with its immunity to burst-errors due to intensity fluctuations make OFDM an interesting candidate for FSO transmission. Recently we have shown [5], [11-12] that significant performance improvement can be obtained by using low-density parity-check (LDPC) codes and iterative decoding based on a sum-product algorithm that does not require knowledge of the joint temporal probability distribution functions. LDPC codes have been shown to achieve impressive coding gains for a variety channels [11-12]. They perform significantly better than turbo-product and Reed-Solomon (RS) codes in bursty-error channels such as the fiber optics communication channel at 40 Gb/s or above [11-12] and the FSO channel [5]; making them an excellent error control coding scheme to combine with OFDM.

In this paper we propose an LDPC coded free-space optical OFDM (FSO-OFDM) system built using standard optical and RF components. The key idea is to lower the symbol rate by using OFDM, and, in combination with interleaving and LDPC codes, to obtain high tolerance to the deep fades that are inherent to a turbulent channel. On the other hand, OFDM is more sensitive to phase noise, and has a relatively large peak-to-average power ratio [6]; so a careful design is needed in order to fully exploit the advantages and minimize the side effects of OFDM. In particular we note that the use of OFDM in the IM/DD system is not very power efficient if implemented as suggested in [14]. To improve the power efficiency, we introduce single-side band clipped- and unclipped-OFDM schemes.

The paper is organized as follows. The concept of FSO-OFDM transmission is introduced in Section 2, the simulation model and error control coding scheme are described in Sections 3 and 4 respectively; while, the numerical results are presented in Section 5. Section 6 concludes the paper.

2. FSO-OFDM transmission system

FSO-OFDM systems support high data rates by splitting a high-rate data-stream into a number of low-rate data-streams and transmitting these over a number of narrowband subcarriers. The narrowband subcarrier data-streams experience smaller distortions than high-speed ones and require no equalization. Moreover, most of the required signal processing is performed in the RF domain. This is advantageous because microwave devices are much more mature than their optical counterparts and because the frequency selectivity of microwave filters and the frequency stability of microwave oscillators are significantly better than that of corresponding optical devices. Furthermore, the phase noise levels of microwave oscillators are significantly lower than that of distributed feedback (DFB) laser diodes, which means that RF coherent detection is easier to implement than optical coherent detection. This, in turn, allows a system architect to directly apply the most advanced coherent modulation formats already developed for wireless communication.

The basic FSO-OFDM transmitter and receiver configurations are shown in Fig. 1(a) and 1(b) respectively. The corresponding FSO link is shown in Fig. 1(c). A 10-Gb/s information-bearing stream is demultiplexed into four 2.5-Gb/s streams, each encoded by identical LDPC encoders (for an example of current available LDPC chips see [19]). The LDPC encoded outputs are further demultiplexed, and parsed into groups of B bits. The B bits in each group (frame) are subdivided into K subgroups with the i^{th} subgroup containing b_i bits, $B=\sum_{i=1}^{K} b_i$. The b_i bits from the i^{th} subgroup are mapped into a complex-valued signal from a 2^{b_i}-point signal constellation such as quadrature-amplitude modulation (QAM), which is considered in this paper. The complex-valued signal points from K subchannels are considered to be the values of the discrete Fourier transform (DFT) of a multicarrier OFDM signal (for more details see Ref. [6]). Therefore, the symbol length (the time between two consecutive OFDM symbols) in an OFDM system is $T=KT_s$, where T_s is the symbol-interval length in an equivalent single-carrier system. By selecting K, the number of subchannels, sufficiently large, the OFDM symbol interval can be made significantly larger than the dispersed pulse-width in a single-carrier system, resulting in an arbitrarily small intersymbol interference.

#79874 - $15.00 USD Received 7 Feb 2007; revised 30 Apr 2007; accepted 30 Apr 2007; published 8 May 2007

Following the description given in Ref. [6], the complex envelope of a transmitted OFDM signal can be written as

$$s(t) = s_{\mathrm{OFDM}}(t) + b, \tag{1}$$

where

$$s_{\mathrm{OFDM}}(t) = \mathrm{Re}\left\{ \sum_{k=-\infty}^{\infty} w(t-kT) \sum_{i=-N_{\mathrm{FFT}}/2}^{N_{\mathrm{FFT}}/2-1} X_{i,k} \cdot e^{j2\pi \frac{i}{T_{FFT}}\cdot(t-kT)} e^{j2\pi f_{RF} t} \right\}$$

is defined for

$$kT - T_{\mathrm{G}}/2 - T_{\mathrm{win}} \le t \le kT + T_{\mathrm{FFT}} + T_{\mathrm{G}}/2 + T_{\mathrm{win}}.$$

In the above expression $X_{i,k}$ denotes the k-th OFDM symbol in the i-th subcarrier, $w(t)$ is the window function, and f_{RF} is the RF carrier frequency. The duration of the OFDM symbol is denoted by T, while T_{FFT} is the FFT sequence duration, T_{G} is the guard interval duration (the duration of cyclic extension), and T_{win} is the length of the windowing interval. The details of the resulting OFDM symbol are shown in Figs. 1(d)-1(e). The symbols are constructed as follows. $N_{\mathrm{QAM}}(=K)$ consecutive input QAM symbols are zero-padded to obtain N_{FFT} $(=2^m, m>1)$ input samples for inverse fast Fourier transform (IFFT), then N_{G} samples are inserted to create the guard interval T_{G} and finally the OFDM symbol is multiplied by the window function (raised cosine function is used in Ref. [6], but the Kaiser, Blackman-Harris and other window functions are also applicable).

The purpose of the cyclic extension is to preserve the orthogonality among subcarriers when the neighboring OFDM symbols partially overlap, and the purpose of the windowing is to reduce the out-of band spectrum. The cyclic extension, illustrated in Fig. 1(d), is performed by repeating the last $N_{\mathrm{G}}/2$ samples of the FFT frame (of duration T_{FFT} with N_{FFT} samples) as the prefix, and repeating the first $N_{\mathrm{G}}/2$ samples (out of N_{FFT}) as the suffix. (Notice that windowing is more effective for smaller numbers of subcarriers.) After a D/A conversion and RF up-conversion, we convert the RF signal to the optical domain using one of two options: (i) for symbol rates up to 10 Gsymbols/s the OFDM signal directly modulates the DFB laser, and (ii) for symbol rates above 10 Gsymbols/s the OFDM signal drives the Mach-Zehnder modulator (MZM). The DC component [b in Eq. (1)] is inserted to enable noncoherent recover of the QAM symbols. In the reminder of this Section three different OFDM schemes are presented.

2.1 Biased-OFDM single-side band scheme

The first scheme is based on intensity modulation, and shall be referred to as the "biased-OFDM" (B-OFDM) scheme. Because bipolar signals cannot be transmitted over an IM/DD link, it is assumed that the bias component b is sufficiently large so that when added to $s_{\mathrm{OFDM}}(t)$ the resulting sum is non-negative. For illustrative purposes the DFB laser driving signal (which is identical to the MZM RF input signal of schemes B and C) is shown in Fig. 2(a). The main disadvantage of the B-OFDM scheme is the poor power efficiency.

2.2 Clipped-OFDM single-side band scheme

To improve the power efficiency we propose two alternative schemes. The first of these, which we shall refer to as the "clipped-OFDM" (C-OFDM) scheme, is based on single-side band (SSB) transmission, with clipping of the negative portion of the OFDM signal after bias addition. The bias is varied to find the optimum one for fixed optical launched power. It was found that the optimum case is one in which ~50% of the total electrical signal energy before clipping is allocated for transmission of a carrier. The MZM RF input signal for C-OFDM scheme is shown in Fig. 2(b).

#79874 - $15.00 USD Received 7 Feb 2007; revised 30 Apr 2007; accepted 30 Apr 2007; published 8 May 2007

2.3 Unclipped-OFDM single-side band scheme

The second power-efficient scheme, which we shall refer to as the "unclipped-OFDM" (U-OFDM) scheme, is based on SSB transmission employing $LiNbO_3$ MZM in a fashion similar to that used in duobinary optical transmission. To avoid distortion due to clipping, the information bearing signal is transmitted by modulating the electrical field (instead of intensity modulation employed in the B-OFDM and C-OFDM schemes) so that the negative part of the OFDM signal is transmitted to the photodetector. Distortion introduced by the photodetector, caused by squaring, is successfully eliminated by proper filtering, and the recovered signal distortion is insignificant. Notice that U-OFDM is less power efficient than C-OFDM because the negative portion of the OFDM signal is transmitted and then discarded [see Fig. 2(c)]. For U-OFDM the detector nonlinearity is compensated by post-detection filters that reject (potentially useful) signal energy and compromise power efficiency. Despite this drawback we find that U-OFDM is still significantly more power efficient than B-OFDM. Note that the DC bias shifts the average of the C-OFDM signal towards positive values, while in the case of B-OFDM a much larger bias is needed to completely eliminate the negative portion of the signal. The MZM RF input signal for U-OFDM is shown in Fig. 2(c), and the recovered constellation diagram for 16-QAM SSB is shown in Fig. 2(g). The transmitted signal is recovered with negligible distortion.

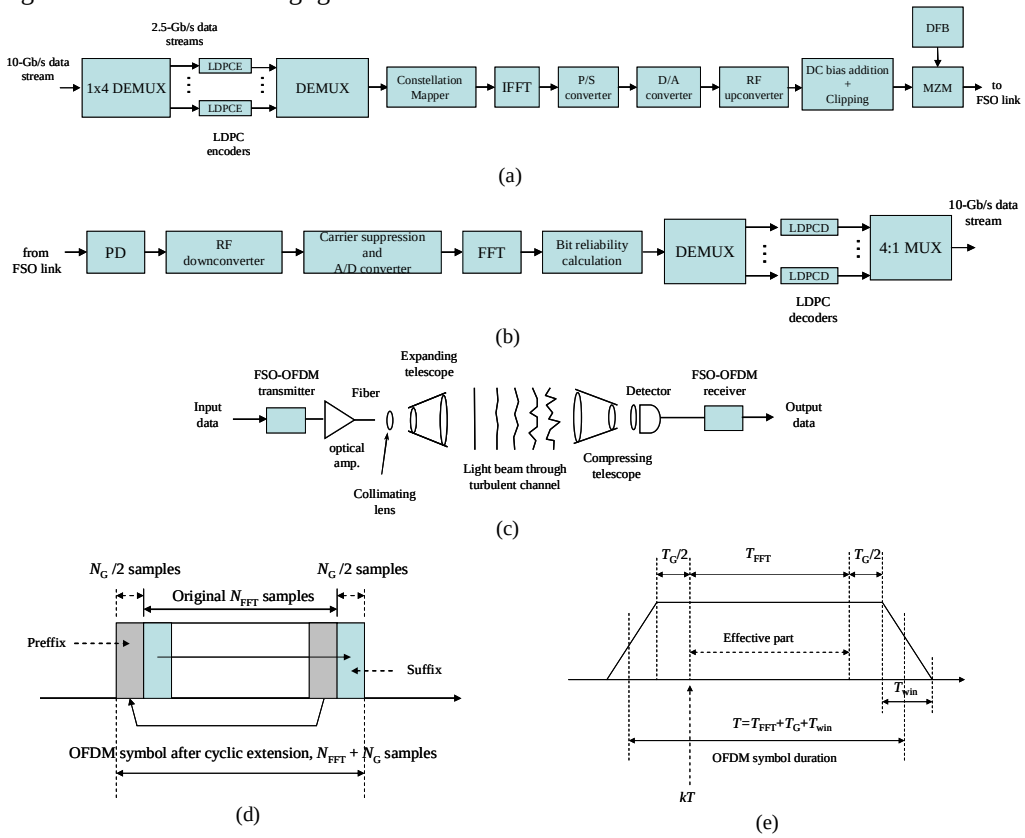

Fig. 1. FSO-OFDM system: (a) transmitter configuration, (b) receiver configuration, (c) FSO link, (d) OFDM symbol cyclic extension, (e) OFDM symbol after windowing. LDPCE-LDPC encoder, LPDCD-LDPC decoder, DFB-distributed-feedback laser, MZM-Mach-Zehnder modulator, S/P-serial-to-parallel, P/S-parllel-to-serial.

#79874 - $15.00 USD Received 7 Feb 2007; revised 30 Apr 2007; accepted 30 Apr 2007; published 8 May 2007

The point-to-point FSO system considered here, shown in Fig. 1(c), consists of an FSO-OFDM transmitter, propagation medium and an FSO-OFDM receiver. The modulated beam is projected toward the receiver using the expanding telescope. At the receiver, an optical system collects the light, and focuses it onto a detector, which delivers an electrical signal proportional to the incoming optical power. Notice that no aperture averaging is applied. The receiver commonly employs the transimpedance design, which is a good compromise between noise and bandwidth. A PIN photodiode plus preamplifier or an avalanche photodiode are typically used as optical detectors. During propagation through the air, the optical beam experiences amplitude and phase variations caused by scattering, refraction caused by atmospheric turbulence, absorption, and building sway. The photodiode output current can be written as

$$i(t) = \mathsf{R}\left|a(t)s_{\mathrm{OFDM}}(t) + a(t)b\right|^2 = \mathsf{R}\left[\left|a(t)s_{\mathrm{OFDM}}(t)\right|^2 + \left|a(t)b\right|^2 + 2R_e\left\{a(t)s_{\mathrm{OFDM}}(t)a^*(t)b\right\}\right], \quad (2)$$

where $|a(t)|^2$ denotes the intensity fluctuation due to atmospheric turbulence, and R denotes the photodiode responsivity. The signal after RF down-conversion and appropriate filtering, can be written as

$$r(t) = \left[i(t)k_{RF}\cos\left(\omega_{RF}t\right)\right] * h_e(\tau) + n(t), \quad (2)$$

where $h_e(t)$ is the impulse response of the low-pass filter (having the transfer function $H_e(j\omega)$), $n(t)$ is electronic noise in the receiver, commonly modeled as a Gaussian process, k_{RF} denotes the RF downconversion factor, and the $*$ is the convolution operator. Finally, after the A/D conversion and cyclic extension removal, the transmitted signal is demodulated by the FFT algorithm. The soft outputs of the FFT demodulator are used to estimate the bit reliabilities that are fed to four identical LDPC iterative decoders based on the sum-product algorithm [15].

#79874 - $15.00 USD Received 7 Feb 2007; revised 30 Apr 2007; accepted 30 Apr 2007; published 8 May 2007

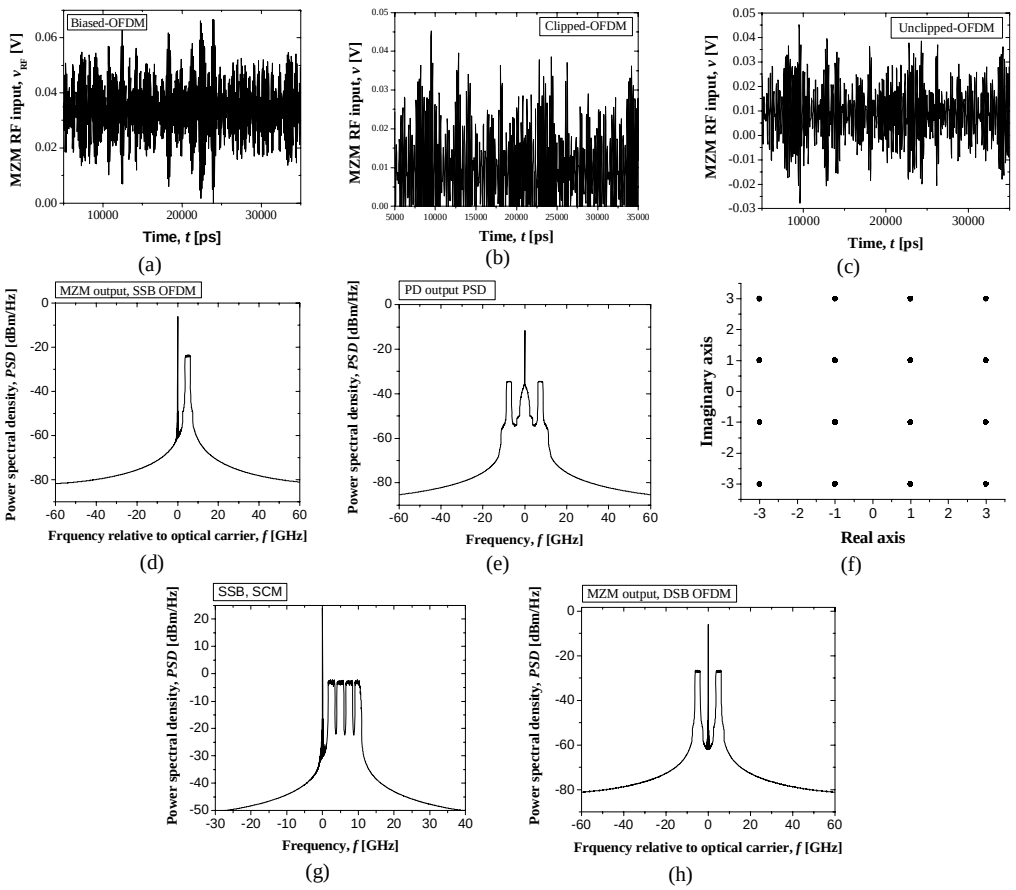

Fig. 2. Waveforms and power spectral densities of the SSB OFDM signal with 64 sub-carriers at different points during transmission of an OFDM signal in a back-to-back configuration: (a) MZM RF input for B-OFDM, (b) MZM RF input for C-OFDM, (c) MZM RF input for U-OFDM, (d) PSD after MZM (U-OFDM), (e) photodectector (PD) output PSD (U-OFDM), (f) receiver constellation diagram for 16-QAM (U-OFDM), (g) PSD of SCM signal with four OFDM channels (U-OFDM). The PSD of double-side band OFDM signal after MZM is shown in Fig. 2 (h) (U-OFDM).

The parameters of the overall OFDM-FSO system must be carefully chosen, as explained later in this section, so that the reconstructed sequence constellation diagram suffers minimal distortion in a back-to-back configuration (when the influence of the channel is neglected).

For the sake of illustration, consider the signal waveforms and power-spectral densities (PSDs) at various points in the OFDM system given in Fig. 2. These examples were generated using SSB transmission in a back-to-back configuration. The bandwidth of the OFDM signal is set to 2.5 GHz, and the RF carrier to 7.5 GHz. The number of OFDM sub-channels is set to 64. The OFDM sequence is zero-padded and the FFT is calculated using 128 points. The guard interval is obtained by a cyclic extension of 2x16 samples as explained above. The windowing (2x16 samples) is based on the Blackman-Harris windowing function. The average transmitted launched power is set to 0dBm. The RF driver amplifier and MZM operate in linear regime [see Figs. 2(a)-2(c)]. The PSD for an SSB OFDM MZM output signal is shown in Fig. 2(d), and the photodetector output signal (for SSB OFDM transmission) is shown in Fig. 2(e). The OFDM term after beating in the PD [the third term in Eq. (2)], the low-pass term, and the squared OFDM term [the first term in Eq. (2)] can easily be identified.

If a 16-QAM OFDM system employing 64 sub-carriers is used in combination with 39 Mb/s sub-channels, the OFDM system proposed here allows transmitting a 10 Gb/s signal

#79874 - $15.00 USD Received 7 Feb 2007; revised 30 Apr 2007; accepted 30 Apr 2007; published 8 May 2007

over a 2.5 GHz bandwidth, thereby increasing the spectral efficiency of OOK. To improve the spectral efficiency further, OFDM may be combined with sub-carrier multiplexing (SCM) in a similar fashion as proposed for fiber-optic communication [16]. In this case [PSD shown in Fig. 2(g)] the spectral efficiency of 4×10Gb/s/11.25GHz =3.55bits/s/Hz is achieved, which is significantly better than that for OOK transmission over an FSO link. (For illustrative purposes, the PSD of DSB OFDM signal is also provided [see Fig. 2(h)].

This high-level description of the system allows us now to introduce a statistical model of atmospheric turbulence based on gamma-gamma distribution (Section 3), and an efficient LDPC error correction scheme based on block-circulant LDPC codes suitable for combining with OFDM (Section 4).

3. An atmospheric turbulence model

One turbulence model that is commonly used in the literature assumes that the variations in medium temperature and pressure due to solar heating and wind can be understood as individual cells of air or eddies of different diameters and refractive indices [1-5]. These eddies may be considered as lenses randomly refracting the optical wave front, and producing a distorted intensity profile at the receiver side of an FSO communication link. The most widely accepted theory of turbulence is due to Kolmogorov [5], and it assumes that kinetic energy from large turbulent eddies, characterized by the outer scale L_0, is transferred without loss to eddies of decreasing size down to sizes of a few millimeters characterized by the inner scale l_0. The inner scale represents the cell size at which energy is dissipated by viscosity. The refractive index varies randomly across the different turbulent eddies and causes phase and amplitude perturbations to a propagating optical wave front. Turbulence can also cause random drifts of optical beams–a phenomenon usually referred to as wandering – and can induce beam focusing. In our study it is assumed that the outer scale is infinite, and that the inner scale is zero; however, it straightforward to extend this analysis to the case of non-zero inner scale [2, 5]. To quantify the strength of the turbulence we use the unitless Rytov variance, given by [5]

$$\sigma_R^2 = 1.23\, C_n^2\, k^{7/6} L^{11/6}, \tag{4}$$

where $k = 2\pi/\lambda$ is the optical wave number, λ is the wavelength, L is the propagation distance, and C_n^2 is the refractive index structure parameter, which we assume to be constant for horizontal paths. Although the Rytov variance represents the scintillation index of an unbounded plane wave in the weak turbulence regime, it can also been used as an intuitive measure of turbulence strength that brings together all relevant physical parameters. Throughout the paper we often refer to σ_R simply as the turbulence strength. The refractive index structure parameter C_n^2 varies from about 10^{-17} $m^{-2/3}$ for very weak turbulence to about $10^{-13} m^{-2/3}$ for strong turbulence [1, 5].

In order to characterize the FSO channel from a communication theory perspective the irradiance is factored into the product of two independent random processes representing the large-scale and small-scale irradiance fluctuations, both with Gamma distributions [2]. The resulting probability density function (PDF), known as the gamma-gamma distribution, can be written as [2]:

$$f(I) = \frac{2(\alpha\beta)^{(\alpha+\beta)/2}}{\Gamma(\alpha)\Gamma(\beta)} I^{(\alpha+\beta)/2-1} K_{\alpha-\beta}\left(2\sqrt{\alpha\beta I}\right),\ I > 0, \tag{5}$$

where I is the signal intensity, $\Gamma(\cdot)$ is the gamma function, and $K_{\alpha-\beta}(\cdot)$ is the modified Bessel function of the second kind and order $\alpha-\beta$. α and β are parameters of the PDF describing the scintillation experienced by plane waves, and in the case of zero-inner scale ($l_0 = 0$) are given by [2]

$$\alpha = \left(\exp\left[\frac{0.49\sigma_R^2}{(1+1.11\sigma_R^{12/5})^{7/6}} \right] - 1 \right)^{-1}, \quad \beta = \left(\exp\left[\frac{0.51\sigma_R^2}{(1+0.69\sigma_R^{12/5})^{5/6}} \right] - 1 \right)^{-1}, \tag{6}$$

#79874 - $15.00 USD Received 7 Feb 2007; revised 30 Apr 2007; accepted 30 Apr 2007; published 8 May 2007

where σ_R^2 is the Rytov variance as given in (4). The PDF parameters α and β represent the effective number of large-scale and small-scale cells, respectively [2]. Therefore, the PDF of the intensity fluctuations at the receiver can be predicted from the physical turbulence conditions. The predicted distribution matches very well the distributions obtained from numerical propagation models [2], ranging from weak turbulence (when it resembles the log-normal distribution) to the strong turbulence regime.

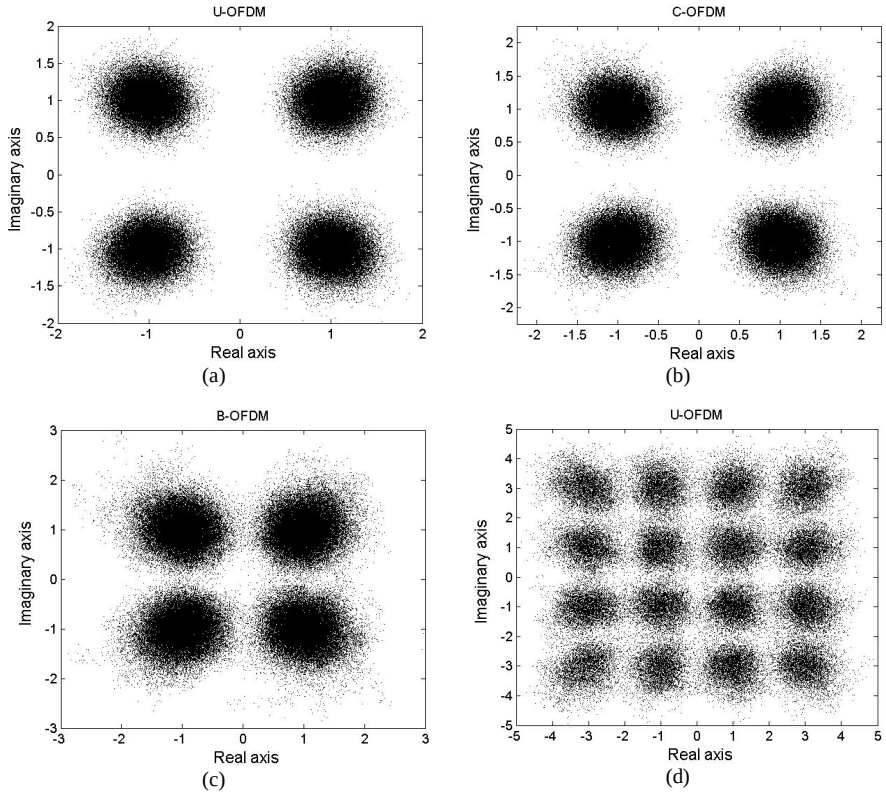

Fig. 3. Received constellation diagrams of QPSK (a)-(c) and 16-QAM (d) SSB FSO-OFDM systems with electrical SNR per bit of 18 dB under the weak turbulence (σ_R=0.6) for: (a),(d) U-OFDM scheme, (b) C-OFDM scheme, and (c) B-OFDM scheme.

The influence of both the atmospheric turbulence and electronic noise on QPSK and 16-QAM SSB FSO-OFDM systems is illustrated in Fig. 3. Results for an SSB OFDM system with 64 sub-carriers are shown. The average launched power is set to 0dBm, the electrical signal-to-noise ratio at the PD is set to 18 dB, and the received signal constellation diagrams are obtained assuming weak atmospheric turbulence (σ_R=0.6). The atmospheric turbulence changes the symmetry of clusters from circular for AWGN channel to elliptic (see Fig. 3). Both C-OFDM and U-OFDM schemes are more immune to the atmospheric turbulence than the B-OFDM scheme. The U-OFDM system is only slightly more immune to the atmospheric turbulence than C-OFDM scheme. It appears that the better power efficiency of C-OFDM compensates the distortion introduced by clipping. The reason is simple. The average launched power is fixed for all three OFDM schemes meaning that more energy per bit is allocated in the C-OFDM scheme (because the power in DC bias is lower), and as a consequence the scheme is more immune to electrical noise. Higher immunity to electrical noise may result in slightly better BER performance of the C-OFDM scheme when compared to the U-OFDM scheme (see Section 5).

#79874 - $15.00 USD Received 7 Feb 2007; revised 30 Apr 2007; accepted 30 Apr 2007; published 8 May 2007

4. Block-circulant LDPC codes and iterative decoding

In this section we give a brief description of the coding scheme used in this paper, as well as an algorithm for calculating the required bit likelihoods in the iterative decoder.

LDPC codes have been shown to significantly outperform turbo-product codes in bursty-error prone channels such as the fiber-optics channel in the presence of intrachannel nonlinear effects [11-12]. The block-circulant LDPC codes similar to those proposed in Ref. [13] are suitable for high-speed implementation because their parity-check matrices have simple cyclic or quasi-cyclic structure, and the encoders can be implemented based on shift registers and modulo 2 adders. As we have shown in Refs. [12-13] the parity-check matrix, $\boldsymbol{H}$, of a regular block-circulant LDPC code can be written as

$$\boldsymbol{H}=\begin{bmatrix} P^{i_1} & P^{i_2} & P^{i_3} & \ldots & P^{i_l} \\ P^{i_l} & P^{i_1} & P^{i_2} & \ldots & P^{i_l-1} \\ \ldots & \ldots & \ldots & \ldots & \ldots \\ P^{i_l-r+2} & P^{i_l-r+3} & P^{i_l-r+4} & \ldots & P^{i_l-r+1} \end{bmatrix}, \quad P=\begin{bmatrix} 0 & 1 & 0 & \ldots & 0 \\ 0 & 0 & 1 & \ldots & 0 \\ \ldots & \ldots & \ldots & \ldots & \ldots \\ 0 & 0 & 0 & \ldots & 1 \\ 1 & 0 & 0 & \ldots & 0 \end{bmatrix},$$

the exponents in $\boldsymbol{H}$ are selected as elements from the following set

$$L=\left\{i: 0\le i\le p^2-1, \theta^i+\theta\in GF(p)\right\}$$

p is a prime, and θ is the primitive element of the finite field GF(p^2). The structure of the parity-check matrix of a block-circulant code facilitates a low-complexity decoder implementation because it is highly regular and only the dimension of the permutation matrix P and the exponents are to be stored. The decoder is based on an efficient realization of the sum-product algorithm given in Ref. [15]. Bit reliabilities fed to the iterative decoder are calculated as explained below.

In FSO communications the receiver electronics noise is commonly modeled as a Gaussian noise (see e.g., [1], [3, 5]). If r_I is the in-phase demodulator sample, and r_Q is the quadrature demodulator sample, then the *symbol* log-likelihood ratio (LLR) is calculated as

$$\lambda\left(\boldsymbol{s}=\left(s_I,s_Q\right)\right)=-\frac{\left(r_I-s_I\right)^2}{2\sigma^2}-\frac{\left(r_Q-s_Q\right)^2}{2\sigma^2}, \tag{7}$$

where s_I and s_Q are the coordinates of a transmitted signal constellation point and AWGN variance (σ^2) is determined from the required electrical signal-to-noise ratio (SNR) per bit E_b/N_o

$$\frac{E_b}{N_o}=\frac{E\left\{\boldsymbol{s}_{i,k}\right\}}{\log_2 M}\frac{P_o}{\sigma^2}. \tag{8}$$

P_o is the normalized received power [6], and $\boldsymbol{s}_{i,k}$ denotes the QAM symbol in the k-th subcarrier channel of the i-th OFDM frame. (With M we denote the number of points in the corresponding constellation diagram.) Notice that the definition of electrical SNR per bit, common in digital communications [Eq. (8)] (see Refs. [6] and [17]), is different from that used in Refs. [1], [3], and [5]. The symbol energy-to-noise density ratio E_s/N_0 is equal to the bit energy-to-noise density ratio E_b/N_0 multiplied by the number of bits per symbol which is typically large. For example, for an OFDM system with 256 sub-carriers using BPSK, E_s/N_0 is about 24 dB larger than E_b/N_0. One must be careful when comparing OFDM system BER performance with OOK, not to confuse the bit energy-to-noise density ratio (E_b/N_0) with symbol energy-to-noise density ratio (E_s/N_0). For more details on OFDM principles the interested reader is referred to Ref. [6], and for more details on comparison of different modulation schemes to Ref. [17].

#79874 - $15.00 USD Received 7 Feb 2007; revised 30 Apr 2007; accepted 30 Apr 2007; published 8 May 2007

The initial *bit likelihoods*, provided to the iterative decoder, are calculated from the symbol LLRs, $\lambda(\boldsymbol{s})$, as

$$L\left(s_j\right) = \log \frac{\sum_{\boldsymbol{s}:s_j=1} \exp\left[\lambda(\boldsymbol{s})\right]}{\sum_{\boldsymbol{s}:s_j=0} \exp\left[\lambda(\boldsymbol{s})\right]}. \tag{9}$$

The Gaussian assumption in Eq. (7) may lead to BER performance degradation because the joint distribution is actually a convolution of the Gaussian and gamma-gamma PDFs. In order to reduce complexity, we use the Gaussian approximation in the calculation of symbol reliabilities. Nevertheless, dramatic performance improvement of an LDPC coded FSO-OFDM system over an LDPC coded FSO OOK system is obtained, as shown in Section 5. In calculating bit reliabilities from symbol ones [Eq. (9)] the following "max-star" operator, defined as $\max^*(x,y)= \log(e^x+e^y)$, is applied recursively [18] $\max^*(x,y)=\max(x,y)+\log(1+e^{-|x-y|})$. Notice that the correction factor $\log\left(1+e^{-|x-y|}\right)$ in $\max^*$-operator for high-speed applications can be either tabulated or even omitted, without significant degradation in performance [18].

5. Simulation Results

Simulation results of an LDPC coded SSB U-OFDM system for two different turbulence strengths are given in Fig. 4. The influence of the atmospheric turbulence channel is included by perturbing the intensities of the OFDM samples (before photodiode) according to the PDF in Eq. (5). Therefore, the worst case scenario is observed. No aperture averaging is applied. For BPSK and QPSK, the coding gain improvement of an LDPC encoded FSO-OFDM system over an LDPC encoded OOK FSO system increases as the turbulence strength increases. However, the 16-QAM FSO-OFDM system is not able to operate in the regime of strong turbulence. For weak turbulence (σ_R=0.6) [see Fig. 4(a)] the coding gain improvement of LDPC coded FSO-OFDM system with 64 sub-carriers over the LDPC encoded FSO OOK system is 8.47 dB for QPSK and 9.66 dB for BPSK, at the BER of 10^{-5}. For strong turbulence (σ_R=3.0) [see Fig. 4(b)] the coding gain improvement of the LDPC coded FSO-OFDM system over the LDPC coded FSO OOK system is 20.24 dB for QPSK and 23.38 dB for BPSK. In both cases the block-circulant [13] LDPC code (4320,3242) of rate 0.75 is employed.

The comparison of different LDPC coded SSB OFDM schemes, under the weak turbulence (σ_R=0.6), is given in Fig. 5. The C-OFDM scheme slightly outperforms the U-OFDM scheme. Both C-OFDM and U-OFDM schemes outperform the B-OFDM scheme by approximately 1.5dB at BER of 10^{-5}.

#79874 - $15.00 USD Received 7 Feb 2007; revised 30 Apr 2007; accepted 30 Apr 2007; published 8 May 2007

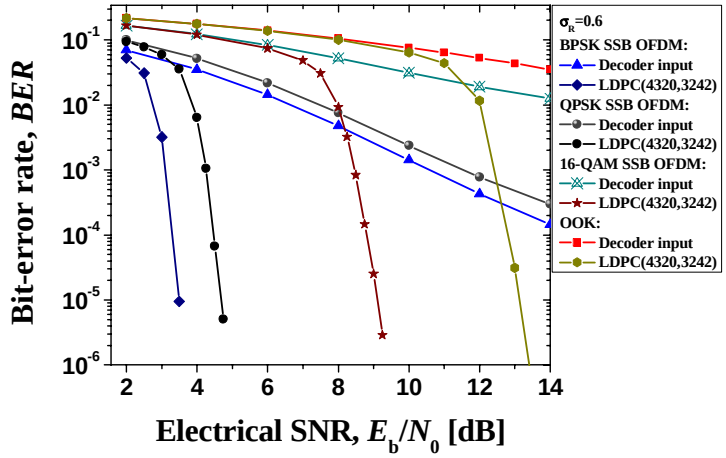

(a)

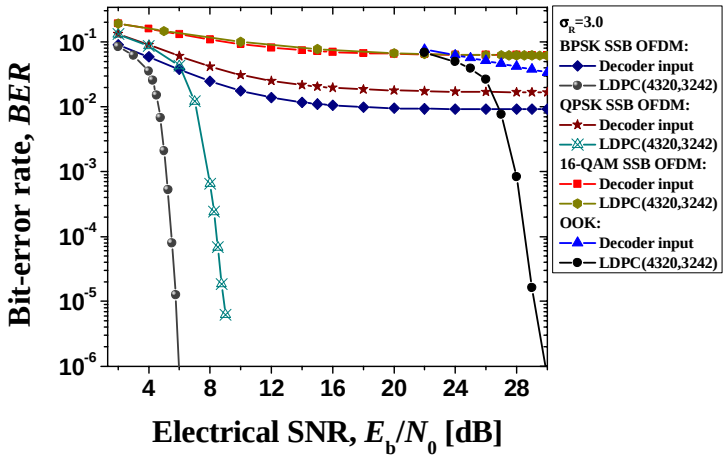

(b)

Fig. 4. BER performance of LDPC-coded SSB U-OFDM system with 64-subcarriers under: (a) the weak turbulence (σ_R=0.6), and (b) strong turbulence (σ_R=3.0).

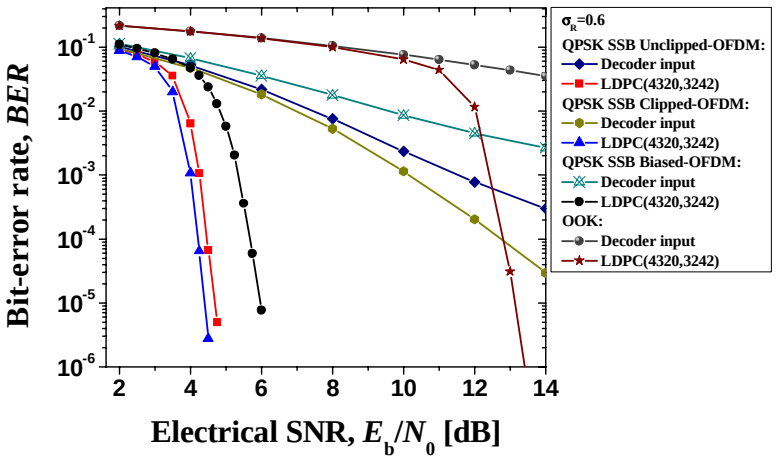

Fig. 5. Comparison of different LDPC coded SSB FSO-OFDM systems with 64-subcarriers under the weak turbulence (σ_R=0.6).

#79874 - $15.00 USD Received 7 Feb 2007; revised 30 Apr 2007; accepted 30 Apr 2007; published 8 May 2007

For the results shown in Figs. 4-5, the received intensity samples are considered to be independent and uncorrelated, similarly as in Refs. [2], [5] and [14]. In reality, especially at high bit rates, the channel has temporal correlation, and consecutive bits propagate experience similar channel conditions. Because of the lack of literature on the temporal statistics in the FSO channel and the complexity of multidimensional joint distributions, we restricted our study (see Figs. 4-5) to the independent and uncorrelated case. In many OFDM systems this approach is reasonable for the following reasons: (i) when the channel conditions do not vary, a simple channel estimation techniques based on pilot signals (see Ref. [6] for more details) can be used to overcome the temporal correlation, and (ii) the immunity to temporal correlation can further be improved by using interleaving. The interleaving can be visualized as the forming an *L*x*N* (*N* is the codeword length) array of *L* LDPC codewords (the parameter *L* is known as interleaving degree) written row by row, and transmitting the array entries column by column.

If the original code can correct a single error burst of length l or less, then the interleaved code can correct a single error burst of length lL. Therefore, interleaved OFDM can successfully eliminate temporal correlation introduced by the FSO channel.

To illustrate the applicability of LDPC-coded OFDM in the presence of temporal correlation we performed simulations by employing the joint temporal correlative distribution model from [1], which describes the fading in an FSO channel at a single point of space at multiple instances of time. This method is based on the Rytov method to derive the normalized log-amplitude covariance function for two positions in a receiving plane perpendicular to the direction of propagation [1], [20]:

$$b_X\left(d_{ij}\right)=\frac{B_X\left(P_i\ ,P_j\right)}{B_X\left(P_i\ ,P_i\right)}, \tag{10}$$

where d_{ij} is the distance between points P_i and P_j. B_X denotes the log-amplitude covariance function:

$$B_X\left(P_i\ ,P_j\right)=E\left[X\left(P_i\right)X\left(P_j\right)\right]-E\left[X\left(P_i\right)\right]E\left[X\left(P_j\right)\right], \tag{11}$$

and X is the log-amplitude fluctuation. The joint temporal distribution of n intensity samples $(I_1,I_2,\ldots,I_n)$ is given by Ref. [1]:

$$f_{\bar{I}}\left(I_1,I_2,...,I_n\right)=\frac{1}{2\pi\prod_{i=1}^{n}I_i}\frac{1}{\left(2\pi\right)^{n/2}\left|C_X\right|^{1/2}}\exp\left[-\frac{1}{8}\left(\ln\frac{I_1}{I_0}...\ln\frac{I_n}{I_0}\right)\right], \tag{12}$$

where C_X is the covariance matrix of intensity samples:

$$C_X=\begin{bmatrix}\sigma_X^2 & \sigma_X^2 b_X\left(\frac{T}{\tau_0}d_0\right) & \ldots & \sigma_X^2 b_X\left(\frac{(n-1)T}{\tau_0}d_0\right)\\ \sigma_X^2 b_X\left(\frac{T}{\tau_0}d_0\right) & \sigma_X^2 & \ldots & \sigma_X^2 b_X\left(\frac{(n-2)T}{\tau_0}d_0\right)\\ \ldots & \ldots & \ldots & \ldots\\ \sigma_X^2 b_X\left(\frac{(n-1)T}{\tau_0}d_0\right) & \sigma_X^2 b_X\left(\frac{(n-2)T}{\tau_0}d_0\right) & \ldots & \sigma_X^2\end{bmatrix}$$

σ^2_X denotes the variance of the log-normally distributed amplitude, which for plane wave can be approximated as Ref. [20]

$$\sigma_X^2\cong 0.56k^{7/6}\int_0^L C_n^2\left(x\right)\left(L-x\right)^{5/6}dx, \tag{13}$$

where the wave number k, propagation length L, and the refractive index structure parameter C_n were introduced earlier. T is the time interval between observations, which corresponds to

#79874 - $15.00 USD Received 7 Feb 2007; revised 30 Apr 2007; accepted 30 Apr 2007; published 8 May 2007

the OFDM symbol period; while τ_0 is the *coherence time*. Notice that expressions (12)-(13) are valid in the *weak* turbulence regime. In the same regime the covariance function (11) is found to be exponential for both plane and spherical waves [20]

$$b_X(\tau) = \exp\left(-\left(\frac{|\tau|}{\tau_0}\right)^{5/3}\right). \tag{14}$$

The typical values of coherence time τ_0 are in the range from 10μs to 10ms.

The results of simulations using the model described by Eq. (12) – Eq. (14) are shown in Fig. 6. The standard deviation σ_X is set to 0.6 (notice that σ_X is different from Rytov standard deviation σ_R used earlier, and for horizontal paths $\sigma_X \sim 0.498\sigma_R$). It is clear from Fig. 6 that LDPC-coded OFDM with or without interleaver provides excellent performance improvement even in the presence of temporal correlation. The BER performance can further be improved by using the interleaver with larger interleaving degree than that used in Fig. 6 (the star curve), at the expense of increasing encoder/decoder complexity. Notice the on-off keying (OOK) modulation scheme enters BER floor for this value of standard deviation (σ_X=0.6), and even advanced FEC is not able to help too much. However, LDPC-coded OOK is able to operate properly at lower standard deviations σ_X.

To generate temporally correlated samples we used two different methods, the first one is based on the Levinson-Durbin algorithm [21], [22], and the second one is based on an algorithm due to Wood and Chan [23].

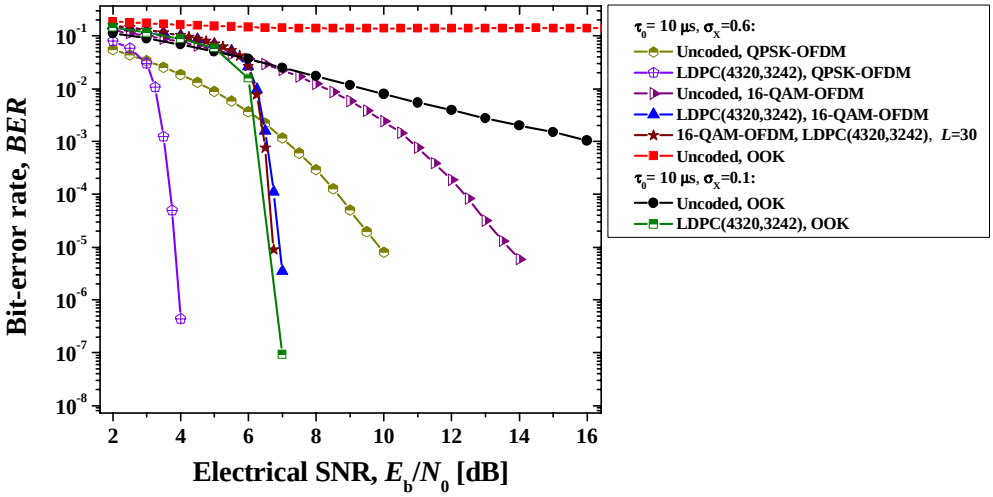

Fig. 6. BER performance of LDPC-coded OFDM in the presence of temporal correlation

6. Conclusion

We have described an LDPC-coded IM/DD-OFDM system, and a novel modulation/coding scheme for FSO systems over atmospheric turbulence channels that provides a number of advantages: (i) excellent coding gains (defined at BER of 10^{-5}) ranging from 8.47 dB in the regime of weak turbulence (for QPSK) to 23.38 dB in the regime of strong turbulence (for BPSK) compared to LDPC-coded OOK, (ii) significant spectral efficiency improvement, (iii) no channel equalization is required, and (iv) a simple FFT is used for modulating and demodulating. To further improve spectral efficiency, the FSO-OFDM SSB transmission scheme may be combined with sub-carrier multiplexing.

#79874 - $15.00 USD Received 7 Feb 2007; revised 30 Apr 2007; accepted 30 Apr 2007; published 8 May 2007

Acknowledgments

This work is funded in part by the NSF under Grant ITR 0325979. The authors would like to thank J. A. Anguita for his involvement in an earlier work on LDPC codes for FSO communication and for useful discussions.

#79874 - $15.00 USD Received 7 Feb 2007; revised 30 Apr 2007; accepted 30 Apr 2007; published 8 May 2007